ADVANCES IN ATMOSPHERIC SCIENCES, VOL. 34, MARCH 2017, 347–359

• **Original Paper** •

A Comparison of Cloud Layers from Ground and Satellite Active Remote Sensing at the Southern Great Plains ARM Site

Jinqiang ZHANG[1,2,3], Xiang'ao XIA[*1,3], and Hongbin CHEN[1,3]

[1]*Key Laboratory of Middle Atmosphere and Global Environment Observation, Institute of Atmospheric Physics, Chinese Academy of Sciences, Beijing* 100029, *China*

[2]*Center of Technical Support and Service, Institute of Atmospheric Physics, Chinese Academy of Sciences, Beijing* 100029, *China*

[3]*Collaborative Innovation Center on Forecast and Evaluation of Meteorological Disasters, Nanjing University of Information Science and Technology, Nanjing* 210044, *China*

(Received 29 January 2016; revised 18 August 2016; accepted 13 September 2016)

ABSTRACT

Using the data collected over the Southern Great Plains ARM site from 2006 to 2010, the surface Active Remote Sensing of Cloud (ARSCL) and CloudSat-CALIPSO satellite (CC) retrievals of total cloud and six specified cloud types [low, mid–low (ML), high–mid–low (HML), mid, high–mid (HM) and high] were compared in terms of cloud fraction (CF), cloud-base height (CBH), cloud-top height (CTH) and cloud thickness (CT), on different temporal scales, to identify their respective advantages and limitations. Good agreement between the two methods was exhibited in the total CF. However, large discrepancies were found between the cloud distributions of the two methods at a high (240-m) vertical grid spacing. Compared to the satellites, ARSCL retrievals detected more boundary layer clouds, while they underestimated high clouds. In terms of the six specific cloud types, more low- and mid-level clouds but less HML- and high-level clouds were detected by ARSCL than by CC. In contrast, the ARSCL retrievals of ML- and HM-level clouds agreed more closely with the estimations from the CC product. Lower CBHs tended to be reported by the surface data for low-, ML- and HML-level clouds; however, higher CTHs were often recorded by the satellite product for HML-, HM- and high-level clouds. The mean CTs for low- and ML-level cloud were similar between the two products; however, the mean CTs for HML-, mid-, HM- and high-level clouds from ARSCL were smaller than those from CC.

Key words: surface, satellite, active remote sensing, cloud

Citation: Zhang, J. Q., X. A. Xia, and H. B. Chen, 2017: A comparison of cloud layers from ground and satellite active remote sensing at the Southern Great Plains ARM site. *Adv. Atmos. Sci.*, **34**(3), 347–359, doi: 10.1007/s00376-016-6030-1.

1. Introduction

Clouds are crucial components of Earth's climate system due to their profound influences on the hydrological cycle and planetary radiation budget by reflecting the incoming solar radiation and absorbing the upwelling infrared radiation (Wang et al., 2014). In addition, the vertical structure and distribution of clouds within the atmosphere interact with atmospheric dynamics (Kalesse and Kollias, 2013). Sherwood et al. (2014) highlighted the importance of low clouds and their feedbacks in the analysis of climate sensitivity. Sassen and Wang (2012) found that mid-level clouds cover about a quarter of Earth's surface and represent a significant contribution to the planet's energy budget. High cirrus clouds often produce a warming effect on the climate system (Huo and Lu, 2014).

A profound knowledge of cloud structure is undoubtedly required for furthering our understanding of cloud climate effects, since these effects are highly dependent on the cloud structure. Unfortunately, cloud profiles are poorly understood at present and remain a primary source of uncertainty in global weather and climate studies (Stephens, 2005). This is mainly because the observation and modeling of cloud profiles is a challenging task, due to the diversity and complexity of cloud distributions, and it is therefore unsurprising that inconsistency exists among different observational and model datasets. To facilitate the use of satellite data to evaluate models in a consistent way, the CFMIP community developed an integrated satellite simulator, COSP (Bodas-Salcedo et al., 2011). By simulating the observations of several satellite-borne active and passive sensors, COSP enables quantitative evaluation of clouds, humidity and precipitation processes in many types of numerical models, from high-resolution models (~1 km resolution) to coarse-resolution models. Another advantage of COSP is that it facilitates model intercompar-

* Corresponding author: Xiang'ao XIA
Email: xxa@mail.iap.ac.cn

© Institute of Atmospheric Physics/Chinese Academy of Sciences, and Science Press and Springer-Verlag Berlin Heidelberg 2017

isons, not only model–satellite comparisons. By taking advantage of the ISCCP simulator, Klein et al. (2013) analyzed the ability of two generations of climate models—nine and ten models' submitted outputs from phases 1 and 2 of CFMIP, respectively—to simulate the climatological distribution of clouds and judge their reliability through comparison to several decades of satellite observations. The results showed that errors in cloud amount as a function of height or climate regime on average presented little or no improvement, although greater improvement could be found in individual models.

The advent of space-borne active cloud radar and lidar has allowed for a better portrayal of cloud vertical structure on the global scale along the curtain of a satellite track, which makes them the most popular instruments in current cloud research (Stephens et al., 2002; Sassen and Wang, 2008). Marchand et al. (2008) described the operational Cloudsat hydrometeor detection algorithm, discussed the difficulties due to surface clutter, and provided a preliminary comparison of the Cloudsat hydrometeor detection algorithm with lidar-based results from the CALIPSO satellite. The authors concluded that, given its limited sensitivity and resolution, as well as surface clutter influences, Cloudsat was unable to detect much of the thin cloud identified by the CALIPSO lidar. By analyzing the first year of millimeter radar data collected by Cloudsat, merged with lidar data collected by CALIPSO (July 2006 to June 2007), Mace et al. (2009) reported that the global hydrometeor coverage averages 76%, and demonstrated a smooth annual cycle with a range of 3% peaking in October 2006 and reaching a minimum in March 2007.

Unlike the space-borne active sensors, ground-based instruments can generate a continuous and long-term cloud climatology at specific locations. For instance, the U.S. DOE's ARM program has deployed a suite of surface remote sensing instruments at a few fixed sites, of which the Southern Great Plains (SGP) site near Lamont, Oklahoma, has been providing observational data over the past two decades. As the first ARM field measurement site, the SGP site is well equipped with a large number of weather and climate research instruments. Furthermore, there are many advantages to this site, such as the relatively homogeneous geography, wide variability of cloud types and surface flux properties, and large seasonal variation in temperature and specific humidity (http://www.arm.gov/sites/sgp). By combining data collected from various ground-based active remote sensing instruments, including radar, ceilometers and lidar, deployed at the SGP site, cloud vertical structure information has been produced and is available as an Active Remote Sensing of Cloud (ARSCL) value-added product (VAP) (Clothiaux et al., 2000). This product has been widely deployed to study the region's cloud characteristics and to evaluate satellite measurements (Kollias et al., 2007; Xi et al., 2010; Qian et al., 2012; Yoo et al., 2013; Kennedy et al., 2014).

Using space-borne and/or ground-based remote sensing cloud products, many studies have been performed to understand cloud processes and evaluate, test, and improve their representations in numerical models at different scales. Zhang et al. (2005) compared the fraction of total, low-level, mid-level and high-level clouds from 10 GCMs with the satellite measurements from ISCCP and CERES program. Although the total cloud amounts agreed well, significant discrepancies existed in the cloud vertical structure among the models, and even between the satellite products. By comparing CMIP5 with CMIP3 and satellite data, Lauer and Hamilton (2013) found that the differences in the simulated cloud climatology from CMIP3 and CMIP5 were generally small, and there was very little to no improvement apparent in the tropical and subtropical regions in CMIP5. To study the role of cloud estimates from satellites in the radiation biases of atmosphere-only simulations of CFMIP2 as part of CMIP5, Bodas-Salcedo et al. (2014) revealed that improving the simulation of mid-level cloud is dominated by two main cloud types: cloud with tops actually at the mid-level, and low-level cloud. They concluded that improving the simulation of these two types should help reduce the biases in simulations of the solar radiation budget over the Southern Ocean in climate models. Dolinar et al. (2015) provided a comprehensive assessment of globally simulated total cloud fraction (CF) from 28 models submitted to CMIP5 as part of AMIP using multiple satellite observations from CERES, MODIS, ISCCP, CloudSat, and CALIPSO during 2000–08. The results showed that the modeled CF was 57.6% and was underestimated by nearly 8% on average when compared to CERES–MODIS and ISCCP results, while an even larger negative bias (17.1%) existed compared to the CloudSat/CALIPSO results.

Now that an increasing number of surface and satellite instruments are providing years of cloud data, a challenging task is to evaluate how consistent the information is from different measurements. In order to reconcile the various sources of cirrus cloud data, Plana-Fattori et al. (2009) conducted a comprehensive comparison of ground-based lidar measurements, and space-borne lidar and sounder data sets. They pointed out that, while some consistencies between the different climatologies were found, the sources of discrepancies were numerous and their effects were not quantified because the datasets were not coincident, and analysis methods were not consistent. In an attempt to evaluate the consistency between the lidar-based cirrus cloud datasets, Dupont et al. (2010) performed a detailed comparison of regional cloud climatologies between four midlatitude ground-based observatories, and spatially and temporally collocated CALIOP observations. It should be noted that they limited the ground-based data to daytime and nighttime hours within ±1.5 h of the nominal satellite overpass times to avoid potential diurnal cycle biases. To obtain enough samples to derive statistics, observations from space-borne lidar were considered within a $2° \times 6°$ latitude–longitude box around the observatory site in their study. The results showed that the consistency in average cloud height (both base and top height) between the CALIOP and ground datasets ranged from −0.4 km to +0.5 km; the cloud geometrical thickness distributions varied significantly between the different datasets, due in part to the original vertical resolutions of the lidar profiles; and the average cloud geometrical thicknesses varied from 1.2 to 1.9 km,

i.e., by more than 50%. The space-borne and ground-based remote sensing cloud products with different viewing geometries (from top-down and from ground-up) have their own merits and respective limitations (Thorsen et al., 2013). Qualitatively, ground-based instruments tend to miss some high cirrus due to the limited lidar detection capability and the signal obscuration by lower-level thick clouds on the radar-lidar sensors (Protat et al., 2014). Satellite measurements should be able to provide a more reliable detection of high cirrus, but they underestimate the clouds formed near the boundary layer because of the attenuation effect (Zhang et al., 2014). Furthermore, other limitations inherent to space-borne instruments include a radar blind zone between the surface and 1 km, and a cloud radar sensitivity of approximately −30 dBZ (Protat et al., 2014).

It has thus far been shown that the variety in viewing geometry, instrument sensitivity and sampling, and observational strategies, among different datasets, will affect their consistency in determining cloud macrophysical and optical property climatologies. In this regard, no single cloud product can be considered as "the truth". A quantitative assessment of their consistency and/or differences is absolutely required. The long-term coexistence of surface and satellite remote sensing measurements over the SGP site presents a unique opportunity to evaluate their performance in detecting the region's clouds at different layers, which is the primary objective of this study. To achieve this, the spatially and temporally collocated cloud estimations in terms of CF, cloud-base height (CBH), cloud-top height (CTH) and cloud thickness (CT), derived from the two approaches, were compared and evaluated in detail on monthly, annual and seasonal temporal scales. More importantly, in view of the fact that clouds in different vertical layers dictate the adiabatic heating rate and the radiation balance of the atmospheric column, the assessment was further conducted for specific cloud types. Following this introduction, section 2 briefly describes the cloud detection algorithms, data and analysis method used in the study. Comparisons of the two cloud products and interpretation of the results are presented in section 3. The main conclusions are summarized in section 4.

2. Data and method

2.1. *Ground-based cloud detection algorithm and product*

Three ground-based active remote sensors [the 35-GHz Millimeter Microwave Cloud Radar (MMCR), Micropulse Lidar (MPL), and laser ceilometers] with vertical resolutions of 45-, 30- and 15-m, respectively, have been deployed at the SGP site (Moran et al., 1998; Clothiaux et al., 1999; Miller et al., 2003). The strengths of these three instruments have been combined to produce the ARSCL VAP with the best possible accuracy (Clothiaux et al., 2000, 2001; Kollias et al., 2009). This cloud product has a temporal resolution of 10 s and a vertical resolution of 45 m; up to 10 cloud layer boundaries can be identified. To calculate the ARSCL-based CF, a similar methodology to Kennedy et al. (2014) was used in this study. A combination of the variables produced by ARSCL VAP was used to derive the combined MMCR+MPL cloud mask for each 10-s, 45-m sample. First, only ARSCL samples with both MMCR detections and MPL columns that were not entirely marked as beam-blocked or attenuated were selected and utilized. Second, cloudy scenes were determined if MMCR or MPL detected clouds. Finally, the best estimate of the cloud base field, using a mixture of ceilometer and MPL information, was deployed to filter hydrometeors below the cloud base. The CF and the occurrence of specific cloud types were obtained on the basis of the above MMCR+MPL cloud mask. The MMCR-based ARSCL data streams at the SGP site ended in January 2011, because the MMCR was out of service and replaced by an upgraded radar called KAZR (Ka-band ARM Zenith-pointing Radar) (Chandra et al., 2015). The ARSCL products generated at the SGP site between 2006 and 2010 were used in this study.

2.2. *Satellite cloud detection algorithm and product*

Two satellites, CloudSat and CALIPSO, were simultaneously launched in April 2006, carrying a 94-GHz cloud profiling radar (CPR) and CALIOP, respectively (Stephens et al., 2002; Winker et al., 2007). Cloudsat uses a near-nadir-pointing millimeter-wavelength radar to probe the vertical structure of clouds and precipitation, while CALIPSO combines an active lidar instrument with passive infrared and visible imagers to probe the vertical structure and properties of thin clouds and aerosols (Marchand et al., 2008). The CPR pulses sample a volume of 480 m in the vertical direction, with an across-track horizontal resolution of 1.4 km. The measured return power, however, is sampled at a rate equivalent to about 240 m in range. CALIOP operates at 532 nm and 1064 nm. The 20-ns laser pulses from CALIOP illuminate a 70-m diameter circle on the ground and the backscattered pulse is sampled with a range resolution of 15 m. Below an altitude of 8.2 km, each 532-nm profile is averaged on board to a vertical resolution of 30 m (Winker et al., 2007). The center-to-center spacing of individual CALIOP profiles is 333 m. Above 8.2 km, the CALIOP data are further averaged horizontally to create a 1-km along-track resolution, and in the vertical direction to create a 60-m resolution. CloudSat and CALIPSO are flown in a tight orbital configuration, allowing them to probe almost equal volumes of the atmosphere within 10–15 s of each other. This configuration, combined with the capacity for millimeter radar to penetrate optically thick hydrometeor layers, and the ability of the lidar to detect optically thin clouds, has allowed us to characterize the vertical and horizontal structure of hydrometeor layers with unprecedented precision (Mace et al., 2009). The combined CloudSat-CALIPSO (CC) cloud mask, which is produced by the official 2B-GEOPROF-LIDAR product derived by combining the two payloads (Mace et al., 2007, 2009), was used in this study to calculate the CF during 2006–10. The vertical grid spacing of the CC cloud mask was 240 m. A complete description of the cloud vertical profile (e.g., the boundaries of up to five cloud layers were identified) is also included in the product (Mace and Zhang, 2014).

2.3. *Collocation of surface and satellite cloud products*

The CC satellites generally overpass the regions surrounding the SGP site twice per day. ARSCL continuously provides cloud vertical profiles over the SGP site in 10-s intervals. The frequencies of cloud occurrence at the CC overpass times are likely to be different from the all-day data obtained by the ground measurements, due to the diurnal cycle of cloud occurrence (Dong et al., 2006; Zhang and Klein, 2010). Hence, the two cloud products should be reasonably matched in both spatial and temporal scales. By conducting sensitivity studies on the PDF of radar reflectivity, CT, and mean vertical profiles of radar reflectivity at the ARM site in Darwin, Australia, Protat et al. (2009) showed that comparing the CC data within a radius of 200 km around the ground-based site with the ground-based data within ±1 h around the satellite overpass of the area, could provide a good trade-off between the need for a large statistical sample and the invariance of cloud properties over the spatial and temporal intervals considered. This collocated methodology of ground-based and satellite active remote sensing data was further employed to compare the cloud frequency of occurrence and associated cloud radiative forcing over the site (Protat et al., 2014). Based on the studies of Protat et al. (2009, 2014), sensitivity studies in terms of vertical CF variations as a function of different radii (200-, 100- and 50 km) for the CC data, and different time windows (±1, ±2 and ±3 h) for the ARSCL data, were conducted at the SGP site in the present study, as shown in Fig. 1. For consistency with the CC product, the vertical resolution of the ARSCL-based MMCR+MPL cloud mask was projected to layers spaced at 240-m intervals from the surface up to the top of the ARSCL profile. The vertical CF was calculated as the number of cloudy occurrences within a specified 240-m grid spacing, divided by the total number of collocated samples during 2006–10. The time window had little impact on the ARSCL-based CF over the SGP site (Fig. 1b); however, the radius (or area) clearly had a large impact on the CC-based CF (Fig. 1a). As stated in Protat et al. (2009), the choice of a maximum distance smaller than 200 km tended to reduce the statistical significance of the CC statistics and introduce more structures in the mean vertical profiles. In view of the results of Protat et al. (2009, 2014), and the vertical CF sensitivity test presented here, a collocation scheme with a radius of 200 km for the CC data and a time window of ±1 h for the ARSCL data was used. The satellites overpass the region surrounding the SGP site at about 0800 UTC and 1900 UTC each day. The CC data within a radius of 200 km around the SGP site (36.6°N, 97.5°W) were selected separately from every satellite overpass. If the selected CC data were available for one particular overpass, the time of the CC sample collected nearest the SGP site was taken as the reference time. The ground-based data were limited to daytime and nighttime hours within ±1 h of this reference time to avoid potential diurnal cycle biases. The collocation process resulted in 544 overpasses; the total number of surface sampling profiles in 10-s intervals was 333 705, which was 2.2 times more than that from the satellite measurements (152 995). When the CFs were calculated, the sample numbers were taken as the percentage of the overpass samples with cloud. The proportions of sample numbers from surface and satellite measurements in Dupont et al. (2010) were 1.5, 0.8, 4.5 and 2.2, at four ground sites, respectively. Hence, based on the studies of Dupont et al. (2010) and Protat et al. (2009, 2014), the collocation method of ground and satellite measurements in our study was deemed reasonable for evaluating the consistency and/or difference between the two datasets in terms of the CF and other macrophysical parameters, such as CBH, CTH and CT.

2.4. *Cloud classification*

To understand how instrument selection and sampling impacts estimates of CF at the SGP site, Kennedy et al. (2014) analyzed 14 years (1997–2010) of cloud observations according to the specific cloud types. To enable comparisons

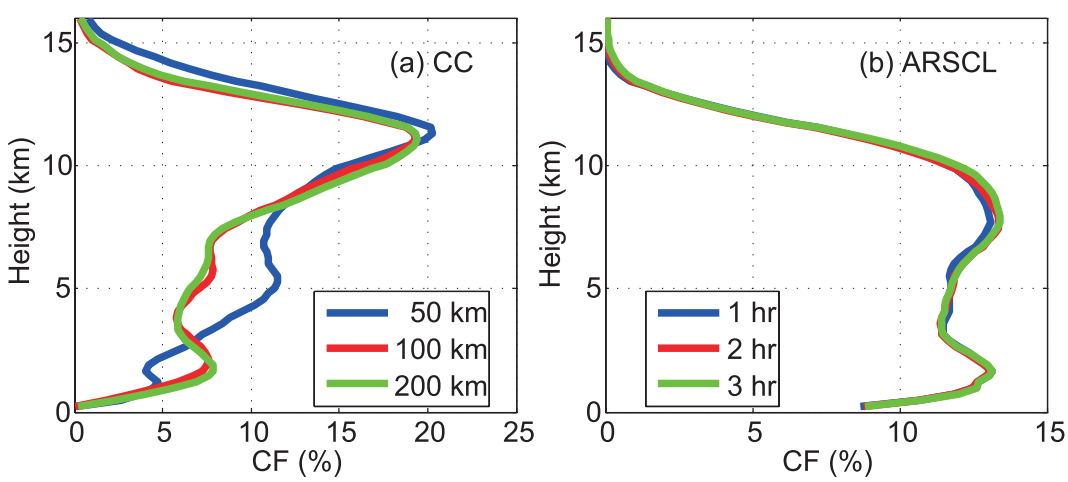

Fig. 1. Assessment of the sensitivity of vertical CF distributions to (a) different radii (50 km, blue line; 100 km, red line; 200 km, green line) for CC data and (b) different time windows (±1 h, blue line; ±2 h, red line; ±3 h, green line) for ARSCL data, during 2006–10.

with ISCCP (Rossow and Schiffer, 1999), they employed a cloud classification system to take advantage of the actively sensed cloud tops and bases, but using a pressure coordinate system. The same cloud classification method was adopted in this study. Switching from a height to pressure coordinate system requires thermodynamic profiles of the atmosphere. In Kennedy et al. (2014), this conversion was accomplished by the information from the archive of Rapid Update Cycle 2 (RUC2) model simulation/analyses covering the region surrounding the SGP site. The number of vertical levels of RUC2 is 40 and its assimilation frequency is 1 h (Benjamin et al., 2004). In this study, a similar methodology to Kennedy et al. (2014) was employed, but utilizing the MergedSounding VAP version 1, rather than RUC2. By combining datasets from radiosonde measurements and the ECMWF, the MergedSounding VAP produces a thermodynamic profile of the atmosphere from the surface to approximately 20 km above ground-level; the vertical resolution varies with height, i.e., 20, 50, 100 and 200 m for altitudes of 0–3, 3–13, 13–16 and 16–20 km, respectively, resulting in 266 vertical levels; the temporal resolution is 1 min. A total of six cloud types [low, mid–low (ML), high–mid–low (HML), mid, high–mid (HM) and high] were classified by converting the CBHs and CTHs to pressures using the MergedSounding data collected over the SGP site, as shown in Fig. 2, adopted from Kennedy et al. (2014). The cloud classes were named by their extension throughout the troposphere (Kennedy et al., 2014), e.g., HML refers to physically thick clouds that extend from pressures higher than 680 hPa (low), through the middle troposphere (mid), and have cloud tops at pressures lower than 440 hPa (high).

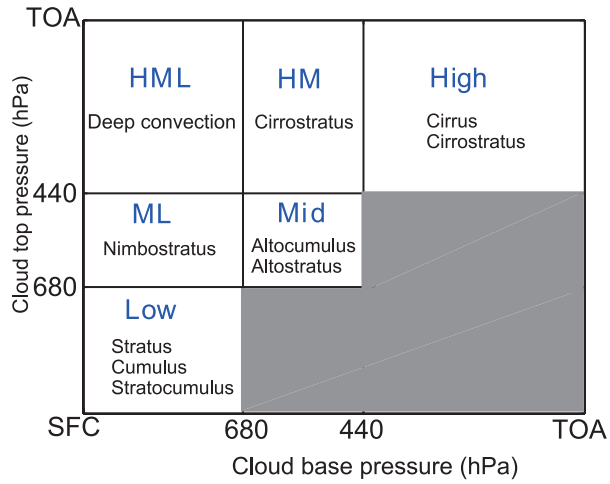

Fig. 2. Schematic representation of the cloud classification system adopted from Kennedy et al. (2014). The blue and black text denotes the six cloud types used in this study and their equivalent ISCCP categories, respectively.

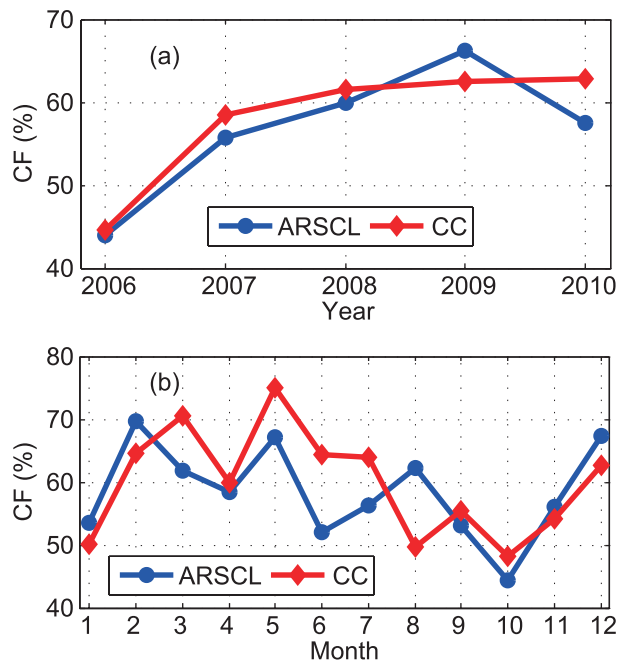

Fig. 3. The (a) annual and (b) monthly total CF derived from the ARSCL (blue line) and CC (red line) products.

3. Comparisons of surface and satellite cloud retrievals

3.1. *Total CF*

The time series (2006–10) of the ARSCL- and CC-based annual/monthly total CF are shown in Figs. 3a and b. The total CF was defined as the number of samples with clouds present anywhere within the whole detecting altitudes, divided by the total number of samples during the year or month in question. The relative occurrence frequencies of the ARSCL and CC samples were close during the same year or month. In general, similar trends in interannual total CF variations were exhibited by the two cloud products, with magnitudes varying between 40% and 70%—especially in 2006, when the CF of the two retrievals were nearly the same (Fig. 3a). The largest difference between the two datasets was 5%, in 2010, when more cloud layers were determined by CC. With regard to monthly distributions, the ARSCL-based CF retrievals closely resembled the CC generations in terms of their variability and gross temporal patterns (Fig. 3b). Overall, more clouds were detected by ARSCL/CC in the first half of the year than the remaining periods. At a more detailed level, it was found that a higher CF tended to be generated by CC than estimated by the ARSCL in several months; their maximum difference was 12% in June.

The annual mean total CF from 2006 to 2010 is presented in Table 1. The CC-based total CF (58% ± 8%) was very close to the ARSCL product (57% ± 8%). Due to the diurnal cycle of cloud occurrence, the ARSCL total CF obtained around the CC overpass time was slightly higher than the value throughout the day (55%) at the SGP site during 1997–2010 (Kennedy et al., 2014). Here, the total cloud layers are discussed extensively on the seasonal scale. The four seasons were defined as follows: winter (December–

Table 1. Yearly and seasonal mean CFs and standard deviations from the ARM ARSCL and CC products during the period 2006–10.

	CF (%)				
	Year	Spring	Summer	Autumn	Winter
ARSCL	57 ± 8	63 ± 3	56 ± 3	53 ± 13	60 ± 13
CC	58 ± 8	69 ± 2	59 ± 4	52 ± 13	57 ± 12

February); spring (March–May); summer (June–August); and autumn (September–November). In general, more cloud layers were detected in spring by ARSCL (63% ± 3%) and CC (69% ± 2%) and fewer layers occurred in autumn. A greater CF was estimated by the ARSCL in autumn and winter, and the reverse was true for spring and summer.

3.2. *Vertical distribution of CF*

Many years' worth of ARSCL and CC data at the SGP site allow for a closer look at the difference in the cloud vertical distribution between the two datasets on different temporal scales. The mean vertical distribution of CF at a grid spacing of 240 m, derived from collocated ground-based MMCR+MPL and CC satellites cloud masks between 2006 and 2010, are shown in Fig. 4; the vertical CFs derived from all ground-based MMCR+MPL cloud masks during the same period at a grid spacing of 45 m and 240 m are also presented. Overall, the shape of the two vertical profiles derived from all ground data was consistent across different vertical scales (45 m and 240 m). Consistent with previous studies (e.g., Wang and Sassen, 2001; Kennedy et al., 2010; Xi et al., 2010), the cloud occurrences at the SGP site were dominated by the clouds in the upper troposphere and in the boundary layer. Meanwhile, the CF increased throughout the troposphere as vertical grid spacing decreased, which was also consistent with the results of Xi et al. (2010) and Kennedy et al. (2014). Compared to the CF distributions from all ground data, slight differences (more boundary layer clouds and less high clouds) tended to occur in the profile from ground data within ±1 h around the satellite overpass, likely associated with the diurnal cycle of cloud occurrence (Dong et al., 2006; Zhang and Klein, 2010). As for the collocated ARSCL- and CC-based CF distributions, although their general patterns were bimodal and similar to some extent, obvious discrepancies existed in their magnitudes. The detecting deficiency of the boundary cloud layers in the CC product indicated the CC failed to detect many near-surface cloud layers. This was mainly due to the contamination of several CloudSat radar bins above Earth's surface by radar ground clutter and the attenuation effect of upper cloud layers on the radar-lidar signals. The ARSCL observations were always larger than the CC retrievals below ~9 km, while the opposite was true above this level. The maximum difference between the two approaches was 12%, at ~12 km, where more high clouds were detected by the satellites. Although close values of total CF were derived from both products (Table 1), there were larger differences for individual cloud layers (Fig. 4), which can be explained as follows. Total cloud appears if clouds in any thin layer within the entire vertical range occur; however, it is extremely likely that a thin cloud is detected by one approach but a thick cloud by the other approach. Hence, it is not surprising that the cloud detection performance differs at a finer vertical resolution between the two approaches. Caution should be taken when these products are used to validate model simulations and passive remote sensing retrievals.

The monthly mean time series of cloud vertical distribution from ARSCL and CC and their difference at a vertical resolution of 240 m are shown in Fig. 5. The monthly relative occurrence frequency of the two kinds of cloud sampling profiles varied from ~6% to ~10%, and was close in magnitude during the same month. The coloring represents the CF (CF difference), in percent, in Figs. 5a and b (Fig. 5c). An obvious difference in cloud occurrence at this finer vertical resolution existed all year between the two cloud products. Substantially more boundary clouds were observed by the ARSCL product. The difference in CF between the two cloud products was >10% at many levels below 2 km, and this feature was largest in February and May, when many low clouds were observed by ARSCL. Another distinct feature was that the ARSCL data missed a significant portion of high cirrus clouds, as compared to the satellite products—especially during May and June, when their difference was ~15% from 10 to 12 km. Overall, the CF of cloud layers in the middle atmosphere from the two observational datasets bore a closer resemblance, as compared to the boundary and high cirrus clouds. However, large discrepancies, with a magnitude around 10%, were still revealed at a few height levels in the middle atmosphere during several months, such as February, May and July.

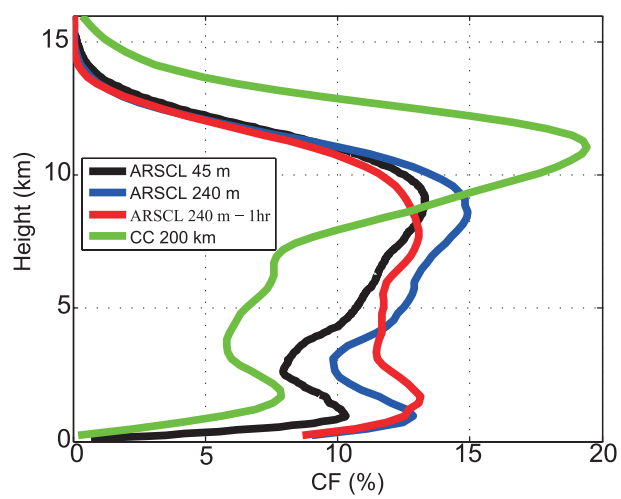

Fig. 4. The vertical CF from ARSCL and CC data during 2006–10. The black and blue lines denote the ARSCL-based CF derived from all MMCR+MPL cloud masks at a grid spacings of 45 and 240 m, respectively. The red and green lines represent the ARSCL- and CC-based CF derived from the collocated MMCR+MPL cloud mask within ±1 hour around the satellite overpass, and the CC cloud mask within a radius of 200 km around the SGP site, respectively; the grid spacing is 240 m.

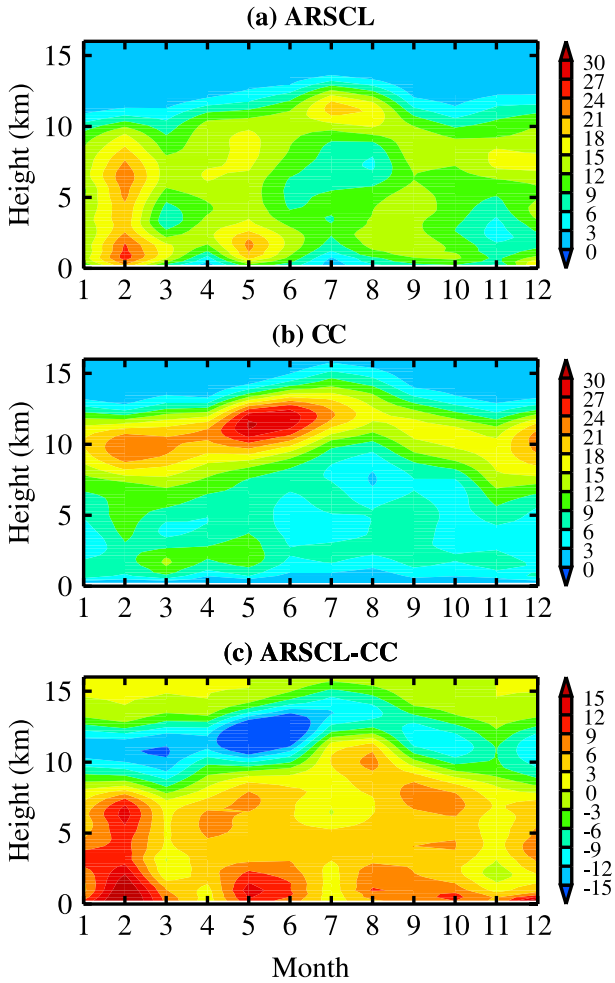

Fig. 5. Monthly mean time series of cloud vertical distribution between 2006 and 2010 from (a) ARSCL and (b) CC, and (c) their differences, spaced at a vertical resolution of 240 m. The coloring represents the CF (units: %) in (a) and (b), and the difference in CF (ARSCL − CC; units: %) in (c).

The mean vertical profiles of cloud distributions from the ARSCL and CC products in the four seasons are shown in Fig. 6. More ARSCL-based boundary cloud layers were observed in spring and winter than in summer and autumn; the maximum CF was more than 15% at 1–2 km in spring and winter. Small frequency values located below 2 km were present in summer because stratus clouds are less frequent during this season (Dong et al., 2005). The satellites detected more high cloud layers in spring, summer and winter than those in autumn. In terms of the cloud layers located between 1 and 2 km, the difference in the cloud retrieval methods was largest in winter, with a maximum of ~9% near 1 km, followed in decreasing order by those in spring, summer and autumn. The difference in cloud layers in the middle atmosphere was generally less than 5%, except in winter when a relatively larger discrepancy existed. Compared to the satellite measurements, high cloud layers located above 10 km were severely underestimated by the ARSCL in spring, with a maximum of ~17% at ~11 km.

3.3. *CFs of six specific cloud types*

The monthly CF distributions of six specific cloud types are shown in Fig. 7. Compared to the CC, ARSCL tended to overestimate the low- and mid-level clouds, but underestimate the HML- and high-level clouds, during most months. By contrast, the ARSCL retrievals of ML- and HM-level clouds agreed more closely with CC. At a more detailed level, it should be noted that, compared to the other four cloud types, relatively larger differences between the two products occurred for low- and high-level clouds, with maxima of 20% and 12% in February and March, respectively. Compared to ARSCL, CC retrieved double the amount of HML clouds during many months. All months were then divided into four seasons to investigate the CF difference between ARSCL and CC on the seasonal scale (see Fig. 8). The CF difference for low-level clouds between the two retrievals hovered around 10%, with a maximum of 11% in summer and minimum of 8% in autumn. A distinct seasonal characteristic of the CF difference was revealed in ML-level clouds: more cloud layers were detected by ARSCL measurements in summer (2%) relative to the CC products, while the opposite was true in spring (−3%), autumn (−2%) and winter (−2%). CC consistently determined more HML-level clouds compared to ARSCL in the four seasons, but with close values that varied between 3% and 4%. The CF difference for mid-level clouds was ~6% in autumn and winter, and ~3% in spring and summer. Compared to the other cloud types, the CF difference for HM-level clouds in the four seasons agreed much more closely, with a magnitude of <1%. An obvious pattern of seasonal variation in the CF difference was found for high-level clouds; the maximum absolute difference occurred in spring (11%), followed by summer (8%), autumn (3%) and winter (3%). The annual mean CFs and their standard deviations for the six specific cloud types over 2006–10 are summarized in Table 2. The absolute difference between the two cloud products was largest for low-level clouds (10%), followed by high- and mid-level clouds (5%), HML-level clouds (4%) and ML-level clouds (1%). The CF of HM-level clouds was the same (7%) for the two approaches.

3.4. *Cloud boundaries and CT*

The locations of cloud boundaries (CBH and CTH) and the distribution of CT have important influences on the thermodynamic structure of the atmosphere and radiation budget of Earth's climate system (Dong et al., 2014). The PDF of the CBH, CTH and CT of total cloud layers derived from the ARSCL and CC products are demonstrated in Fig. 9. The PDF of the ARSCL CBH below 1 km was 17.4%, which was ~7% larger than that of CC (10.0%). In contrast, the PDF of the ARSCL retrieval of the CBH within 1–2 km was 14.1%, which was ~8% less than that of the CC products (21.8%). The PDF of the ARSCL retrieval of the CBH within 3–8 km was slightly larger than that of the CC product. For CBHs>8 km, the PDF of the ARSCL retrieval was slightly smaller. The PDFs of ARSCL CTHs<11 km were generally larger than those of CC. However, obviously larger PDFs of

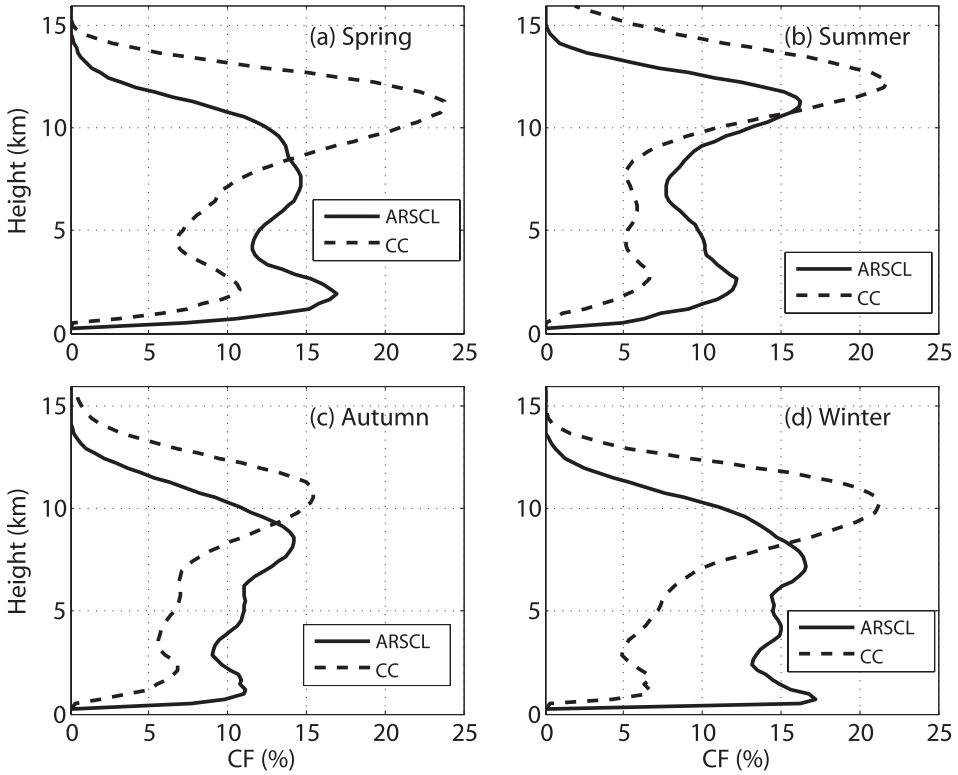

Fig. 6. Average profiles of vertical CF from ARSCL (solid line) and CC (dashed line) in (a) spring, (b) summer, (c) autumn and (d) winter, between 2006 and 2010; the vertical resolution is 240 m.

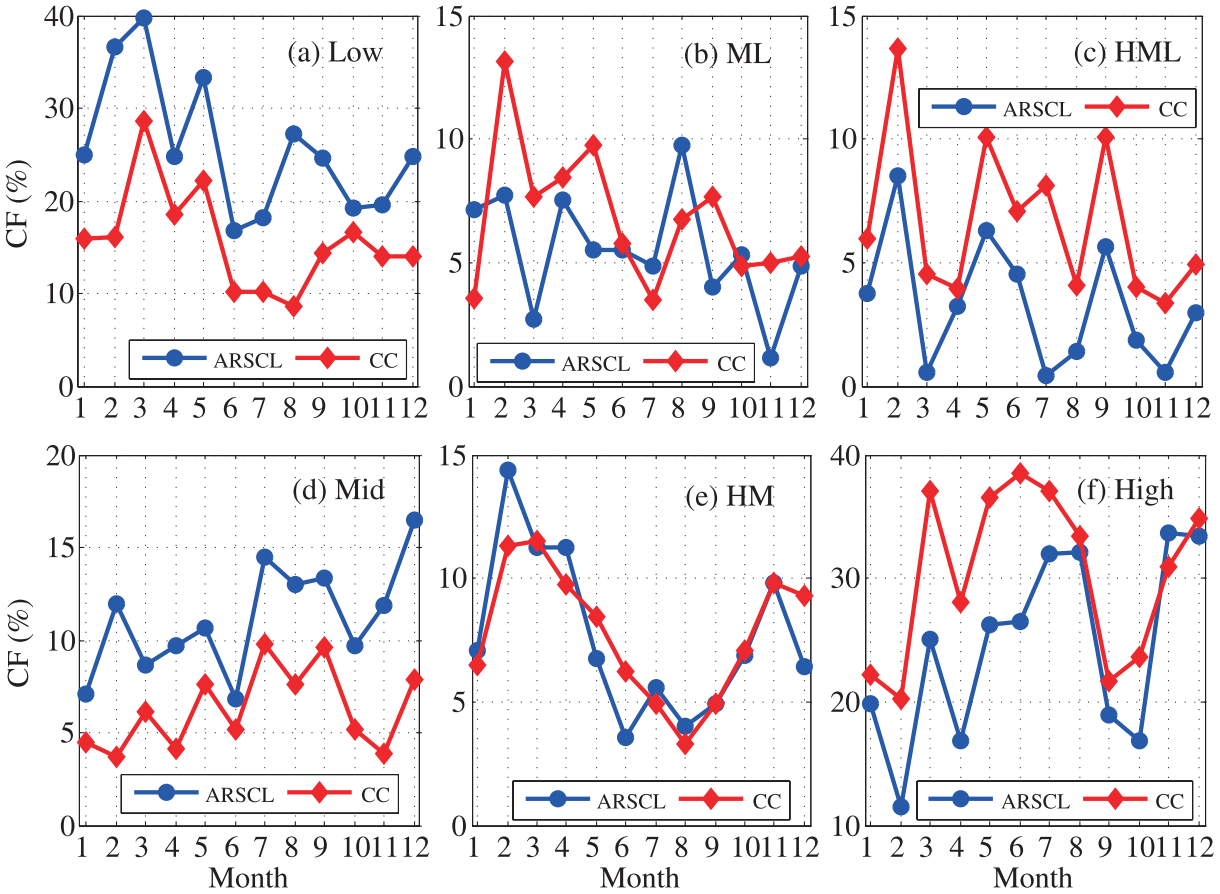

Fig. 7. As in Fig. 3b, but for six specific cloud types: (a) low-level clouds; (b) ML-level clouds; (c) HML-level clouds; (d) mid-level clouds; (e) HM-level clouds; (f) high-level clouds.

Table 2. Mean CFs and CTs and their standard deviations calculated from the ARSCL and CC products during 2006–10 for six specific cloud types.

	CF (%)						CT (km)					
	Low	ML	HML	Mid	HM	High	Low	ML	HML	Mid	HM	High
ARSCL	24 ± 10	5 ± 2	3 ± 1	11 ± 3	7 ± 2	25 ± 3	0.5 ± 0.5	2.5 ± 1.6	8.2 ± 2.1	0.5 ± 0.6	3.5 ± 2.1	1.1 ± 1.0
CC	14 ± 5	6 ± 2	7 ± 2	6 ± 1	7 ± 2	30 ± 3	0.6 ± 0.4	2.5 ± 1.3	9.1 ± 2.8	0.9 ± 0.6	4.2 ± 2.3	2.0 ± 1.4

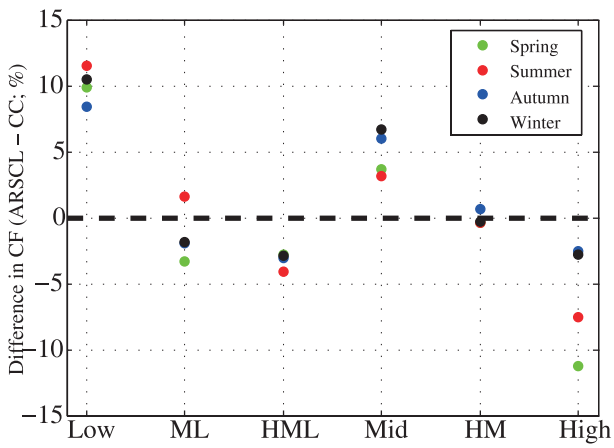

Fig. 8. Seasonal difference in CF between the ARSCL and CC products (ARSCL – CC) for six specific cloud types (categories on the *x*-axis): green dots, spring; red dots, summer; blue dots, autumn; black dots, winter.

CTHs>11 km were derived by CC, with the largest difference being 7.1% at 13 km. Thin cloud layers with CTs <1 km were often observed by ARSCL, with a PDF of 63.8%, which was much larger than that of the CC product (38.3%). Similar structures were then demonstrated by the two cloud retrievals for CTs>1 km, despite systematically larger PDFs for the CC-based CTs relative to the ARSCL estimations. The average CC cloud layer was geometrically thicker (2.5 km) than that of ARSCL (1.3 km) by 1.2 km. The maximum number of cloud layers determined by the ARSCL and CC were ten and five for one particular profile, which likely resulted in more thick cloud layers derived from the satellite data.

The PDFs of CBH spaced at 1 km intervals for the six specific cloud types are shown in Fig. 10. For low-, ML- and HML-level clouds, larger PDF values were produced by ARSCL relative to CC for CBHs<1 km, while the opposite was true within 1–2 km; close PDF magnitudes were then seen for CBHs>2 km. Overall, ARSCL/CC-based CBHs for these three cloud types were most frequently observed below 2 km, accounting for 82%/91%, 46%/61% and 73%/91% for low-, ML- and HML-level clouds, respectively. Excellent agreement between the two cloud retrievals was found for mid-level CBHs; the largest PDF (~80%) of the two methods occurred from 4 to 5 km. In general, similar CBH trends of HM-level clouds were well presented by ARSCL and CC collections, although some differences in magnitude were occasionally seen at a few altitude levels. The vertical structures of CBH for high-level clouds derived from the two methods were similar, and occurred most frequently between 8 and 12 km for ~80% of both retrievals.

Figure 11 illustrates the CTH distributions of the six specific cloud types. For low-level clouds, the ARSCL overestimated and underestimated the CTH relative to the CC data, by 12% below 1 km and by 11% within 1–2 km, respectively; close PDF values were then revealed by the two methods at higher altitudes. Compared to the other cloud types, much better agreement between the ARSCL and CC products was exhibited in ML- and mid-level clouds, with most values around 5 km. A common CTH feature presented

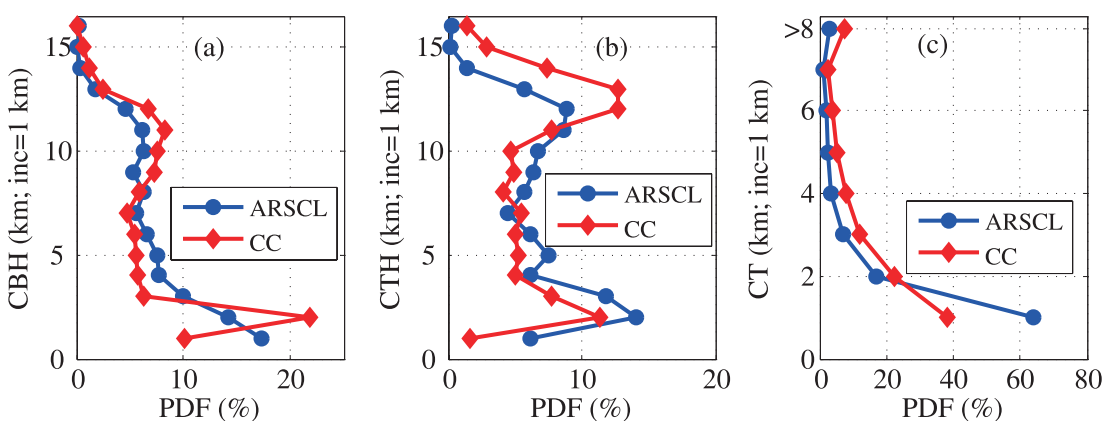

Fig. 9. The PDFs of (a) CBH, (b) CTH and (c) CT derived from ARSCL (blue line) and CC (red line) between 2006 and 2010. The space intervals are 1 km in all three panels.

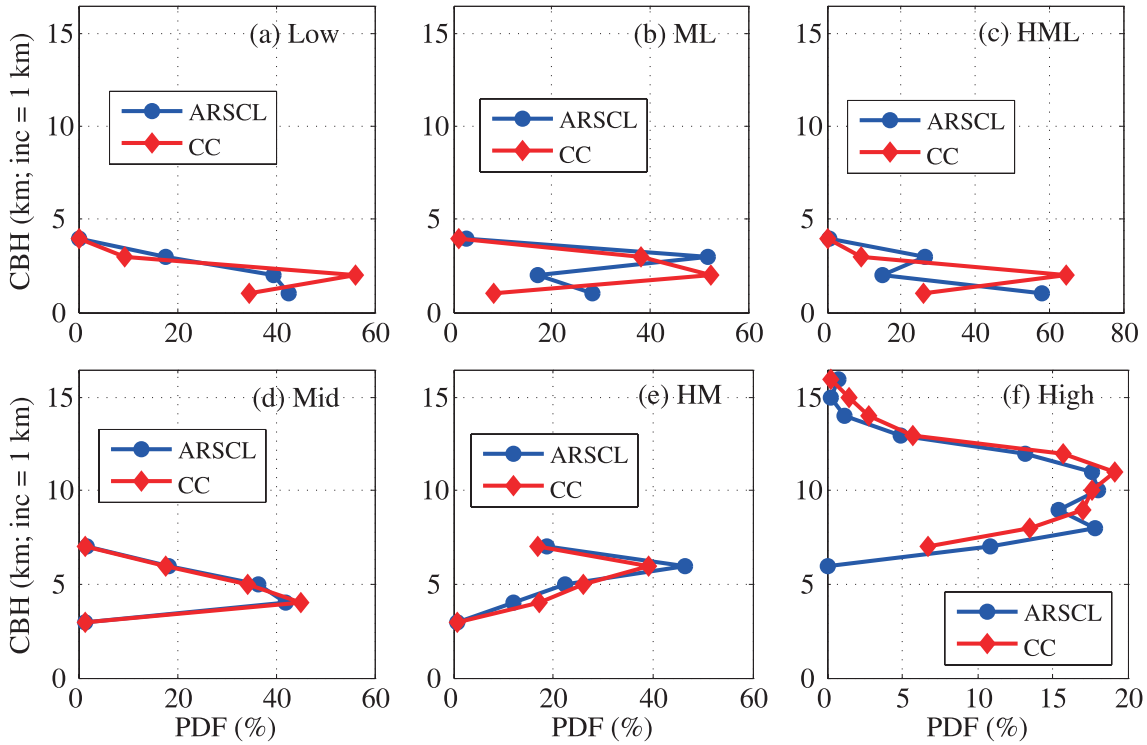

Fig. 10. The PDFs of CBH derived from ARSCL (blue line) and CC (red line) between 2006 and 2010 for six specific cloud types: (a) low-level clouds; (b) ML-level clouds; (c) HML-level clouds; (d) mid-level clouds; (e) HM-level clouds; (f) high-level clouds. The space intervals are 1 km in all panels.

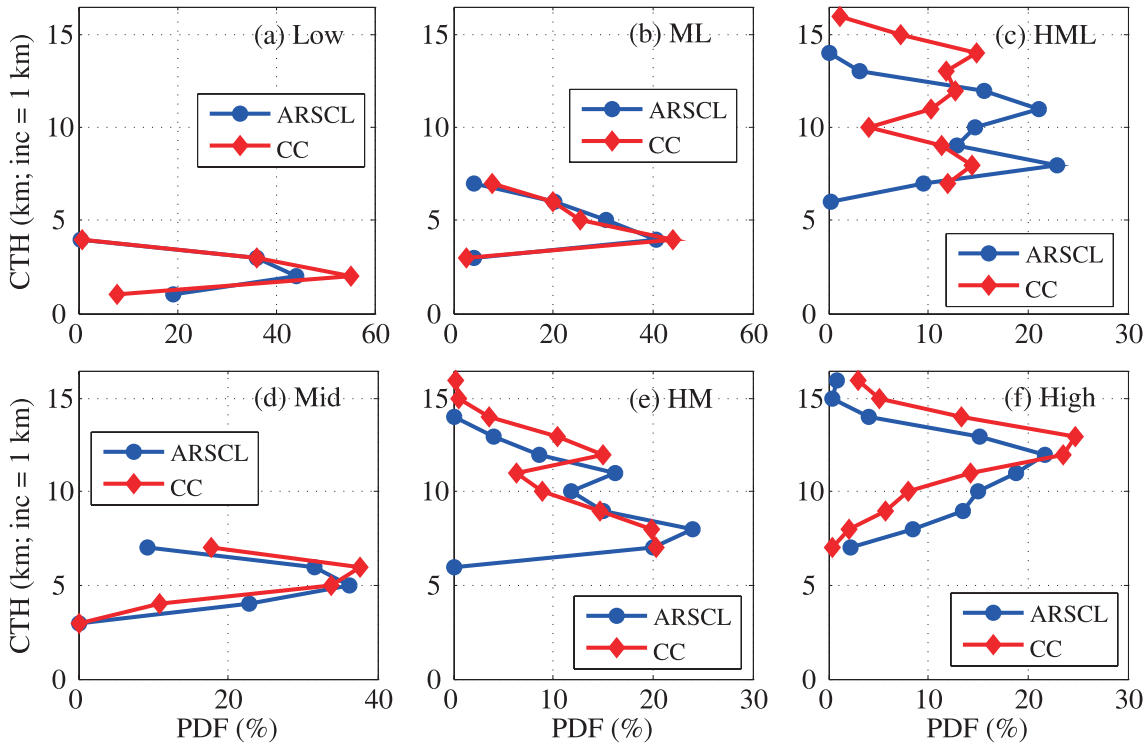

Fig. 11. As in Fig. 10, but for CTH.

in HML-, HM- and high-level clouds was that the CC-based PDF was larger, and placed them higher in the upper atmosphere, than that from the ARSCL measurements, indicating the limitation of surface instruments in detecting the upper clouds. The largest deficiency of ARSCL relative to CC was 15% at 14 km, 6% at 12 km, and 10% at 13 km, for the HML-, HM- and high-level clouds, respectively.

The occurrence frequency of CT spaced at 1-km inter-

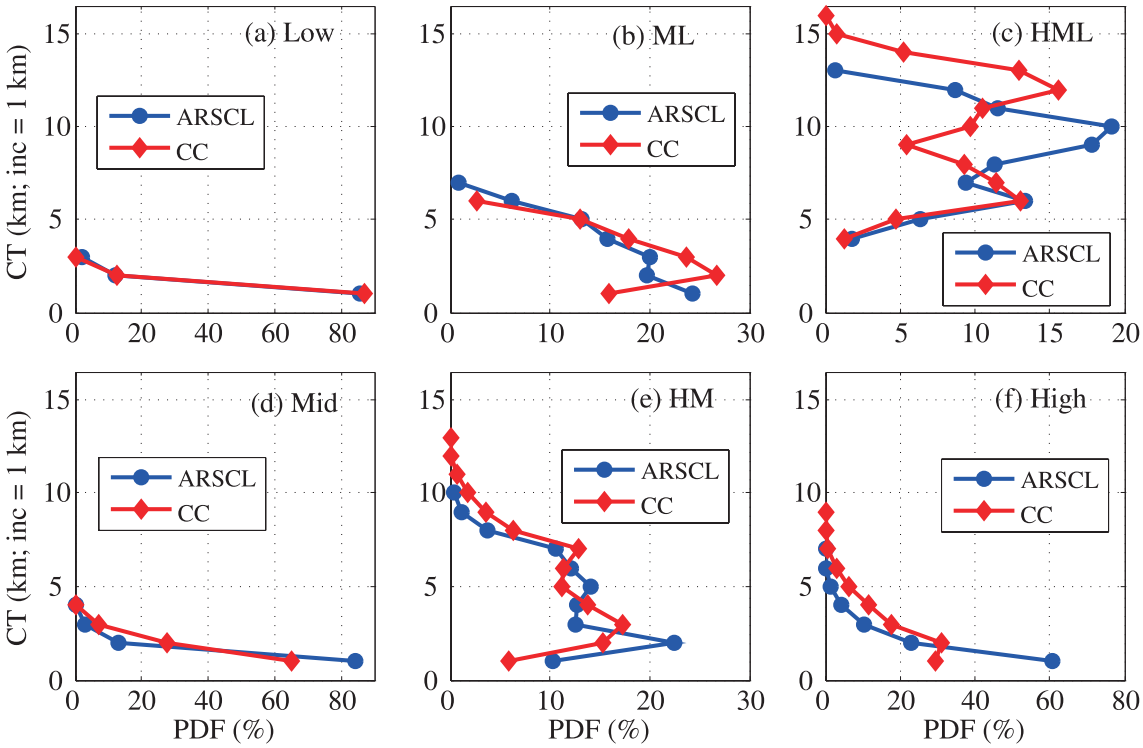

Fig. 12. As in Fig. 10, but for CT.

vals for the six specific cloud types is presented in Fig. 12. Overall, the CT of low-level clouds determined by the two approaches agreed well, and the majority of them were less than 1 km for ARSCL (86%) and CC (87%), respectively. The ML-level clouds were most frequently observed by ARSCL and CC with CTs<4 km, and the PDF value generally varied around 20% at one specific interval between 1 and 4 km. In addition, the PDF of the CC-based CT was larger than that from ARSCL, with a maximum difference of 7% between 2 and 4 km; however, the opposite was true in the other altitude ranges. The ARSCL-based CT occurrence profile for HML-level clouds exhibited a bimodal distribution, with a lower peak (13%) at 6 km and an upper peak (19%) at 10 km. A similar structure was basically presented by CC, except that it placed the upper peak higher than in the ARSCL retrievals. Large discrepancies existed in the CTs of mid-level clouds insofar as that the ARSCL-based PDF was larger in magnitude than the CC product by about 20% for CTs <1 km. Compared to the CC data, the PDF of HM-level clouds derived from ARSCL was greater for CTs below 2 km, close between 3 and 6 km, and then smaller up to the top of the profile. For high-level clouds, most CC-based PDFs were larger than in the ARSCL product, by 3%–8% between 2 and 6 km; however, a notable deficiency in CC estimation of ~30% for CTs<1 km was apparent. The mean CTs and their standard deviations in ARSCL and CC retrievals are summarized in Table 2. The mean CT was close between the two products for low- and ML-level clouds. The average CTs of the ARSCL retrievals were always thinner relative to the CC data for HML-, mid-, HM- and high-level clouds, with differences of 0.9, 0.4, 0.7and 0.9 km, respectively.

4. Conclusion

Accurate information on cloud vertical distributions is vital for meteorological and climate studies, due to the impact of clouds both on Earth's radiation budget and atmospheric adiabatic heating. However, large discrepancies exist among different instruments, which makes it valuable to carefully evaluate observation-based cloud products. By using the cloud products collected over the ARM SGP site from 2006 to 2010, the advantages and limitations of surface and satellite remote sensing methods were evaluated in detail in this study through quantitative assessment of their consistency and/or differences on the monthly, annual and seasonal scales. Meanwhile, the assessment was also conducted according to six specific cloud types: low-, ML-, HML-, mid-, HM- and high-level clouds.

Good agreement between the two methods was found for the mean total CF, which was 57% ± 8% and 58% ± 8% for the ground-based and space-borne products, respectively. However, large differences in the vertical distribution of clouds were exhibited at high grid spacing (240 m). The largest difference in cloud layers between 1 and 2 km from the two datasets was observed in winter, with a maximum of ~9%, followed in decreasing order by the differences in spring, summer and autumn. Differences in the middle cloud layers were generally less than 5%. The performance of the ground-based instruments in detecting high cloud layers deteriorated in spring, with the greatest difference reaching ~17% at ~11

km. The absolute difference in CF between the two cloud products was largest for low-level clouds (10%), followed by high- and mid-level clouds (5%), HML-level clouds (4%) and ML-level clouds (1%); the CF of HM-level clouds was the same (7%) for the two approaches. Larger PDFs of the ARSCL-based CBH at low altitude were exhibited for the low-, ML- and HML-level clouds relative to the CC data; whereas, the PDFs of CC-retrieved CTHs of HML-, HM- and high-level clouds were larger, and placed them higher in the upper atmosphere, than that from the ARSCL measurements. The mean CT was close between the surface and satellite measurements for low- and ML-level clouds; whereas, a larger mean CT was derived from the CC product relative to the ARSCL estimation for the HML-, mid-, HM- and high-level clouds, by 0.9, 0.4, 0.7 and 0.9 km, respectively.

Validation of climate models requires accurate knowledge of cloud macrophysical properties from observational data. The current study shows that, due to instrument limitations and the attenuation effect of thick clouds on the detection capability of instruments, surface measurements tend to underestimate high cirrus clouds and satellite products readily underreport near-surface cloud layers. As such, caution must be exercised when using any one particular product. Combining the strengths of various methods will obtain more reliable cloud retrievals, especially when used for the validation of model outputs.

Acknowledgements. Ground-based measurements from the U.S. DOE's ARM Climate Research Facility located near Lamont, Oklahoma, were used in this study. Satellite data were provided by the CloudSat Data Processing Center at http://www.cloudsat.cira.colostate.edu. This work was supported by the National Natural Science Foundation of China (Grant Nos. 61327810, 41275039, 41675033, and 91337214). The authors thank Aaron D. KENNEDY of the University of North Dakota for his advice on the calculation of ground-based CF. We also thank the two anonymous reviewers, whose suggestions led to a greatly improved manuscript.

REFERENCES

Benjamin, S. G., and Coauthors, 2004: An hourly assimilation-forecast cycle: The RUC. *Mon. Wea. Rev.*, **132**, 495–518.

Bodas-Salcedo, A., and Coauthors, 2011: COSP: Satellite simulation software for model assessment. *Bull. Amer. Meteor. Soc.*, **92**, 1023–1043.

Bodas-Salcedo, A., and Coauthors, 2014: Origins of the solar radiation biases over the southern ocean in CFMIP2 models. *J. Climate*, **27**, 41–56.

Chandra, A., C. Zhang., P. Kollias, S. Matrosov, and W. Szyrmer, 2015: Automated rain rate estimates using the Ka-band ARM Zenith Radar (KAZR). *Atmospheric Measurement Techniques*, **8**, 3685–3699.

Clothiaux, E. E., and Coauthors, 1999: The atmospheric radiation measurement program cloud radars: operational modes. *J. Atmos. Oceanic. Technol.*, **16**, 819–827, doi: 10.1175/1520-0426(1999)016<0819:TARMPC>2.0.CO;2.

Clothiaux, E. E., T. P. Ackerman, G. G. Mace, K. P. Moran, R. T. Marchand, M. A. Miller, and B. E. Martner, 2000: Objective determination of cloud heights and radar reflectivities using a combination of active remote sensors at the ARM CART sites. *J. Appl. Meteor.*, **39**, 645–665.

Clothiaux, E. E., and Coauthors, 2001: The ARM millimeter wave cloud radars (MMCRs) and the active remote sensing of clouds (ARSCL) value added product (VAP). DOE Tech. Memo. ARM VAP-002.1, 38 pp.

Dolinar, E. K., X. Q. Dong, B. K. Xi, J. H. Jiang, and H. Sui, 2015: Evaluation of CMIP5 simulated clouds and TOA radiation budgets using NASA satellite observations. *Climate Dyn.*, **44**, 2229–2247.

Dong, X. Q., P. Minnis, and B. K. Xi, 2005: A climatology of midlatitude continental clouds from the ARM SGP central facility. Part I: Low-level cloud macrophysical, microphysical, and radiative properties. *J. Climate*, **18**, 1391–1410.

Dong, X. Q., B. K. Xi, and P. Minnis, 2006: A climatology of midlatitude continental clouds from the ARM SGP central facility. Part II: Cloud fraction and surface radiative forcing. *J. Climate*, **19**, 1765–1783.

Dong, X. Q., B. K. Xi, A. Kennedy, P. Minnis, and R. Wood, 2014: A 19-month record of marine aerosol-cloud-radiation properties derived from DOE ARM mobile facility deployment at the Azores. Part I: Cloud fraction and single-layered MBL cloud properties. *J. Climate*, **27**, 3665–3682, doi: 10.1175/JCLI-D-13-00553.1.

Dupont, J. C., and Coauthors, 2010: Macrophysical and optical properties of midlatitude cirrus clouds from four ground-based lidars and collocated CALIOP observations. *J. Geophys. Res.*, **115**, D00H24, doi: 10.1029/2009JD011943.

Huo, J., and D. R. Lu, 2014: Physical properties of high-level cloud over land and ocean from *CloudSat-CALIPSO* data. *J. Climate*, **27**, 8966–8978, doi: 10.1175/JCLI-D-14-00329.1.

Kalesse, H., and P. Kollias, 2013: Climatology of high cloud dynamics using profiling ARM Doppler radar observations. *J. Climate*, **26**, 6340–6359.

Kennedy, A. D., X. Q. Dong, and B. K. Xi, 2014: Cloud fraction at the ARM SGP site: instrument and sampling considerations from 14 years of ARSCL. *Theor. Appl. Climatol.*, **115**, 91–105.

Kennedy, A. D., X. Q. Dong, B. K. Xi, P. Minnis, A. D. Del Genio, A. B., Wolf, and M. M. Khaiyer, 2010: Evaluation of the NASA GISS Single-column model simulated clouds using combined surface and satellite observations. *J. Climate*, **23**, 5175–5192.

Klein, S. A., Y. Y. Zhang, M. D. Zelinka, R. Pincus, J. Boyle, and P. J. Gleckler, 2013: Are climate model simulations of clouds improving? An evaluation using the ISCCP simulator. *J. Geophys. Res.*, **118**, 1329–1342.

Kollias, P., G. Tselioudis, and B. A. Albrecht, 2007: Cloud climatology at the Southern Great Plains and the layer structure, drizzle, and atmospheric modes of continental stratus. *J. Geophys. Res.*, **112**, D09116, doi: 10.1029/2006JD007307.

Kollias, P., M. A. Miller, K. L. Johnson, M. P. Jensen, and D. T. Troyan, 2009: Cloud, thermodynamic, and precipitation observations in West Africa during 2006. *J. Geophys. Res.*, **114**, D00E08, doi: 10.1029/2008JD010641.

Lauer, A., and K. Hamilton, 2013: Simulating clouds with Global Climate Models: a comparison of CMIP5 results with CMIP3 and satellite Data. *J. Climate*, **26**, 3823–3845.

Mace, G. G., and Q. Q. Zhang, 2014: The CloudSat radar-lidar geometrical profile product (RL-GeoProf): updates, improvements, and selected results. *J. Geophys. Res.*, **119**, 9441–9462, doi: 10.1002/ 2013JD021374.

Mace, G. G., R. Marchand, Q. Q. Zhang, and G. Stephens, 2007: Global hydrometeor occurrence as observed by CloudSat: initial observations from summer 2006. *Geophys. Res. Lett.*, **34**, L09808, doi: 10.1029/2006GL029017.

Mace, G. G., Q. Q. Zhang, M. Vaughan, R. Marchand, G. Stephens, C. Trepte, and D. Winker, 2009: A description of hydrometeor layer occurrence statistics derived from the first year of merged Cloudsat and CALIPSO data. *J. Geophys. Res.*, **114**, D00A26, doi: 10.1029/2007JD009755.

Marchand, R., G. G. Mace, T. Ackerman, and G. Stephens, 2008: Hydrometeor detection using *Cloudsat*-an earth-orbiting 94-GHz cloud radar. *J. Atmos. Oceanic Technol.*, **25**, 519–533.

Miller, M. A., K. L. Johnson, D. T. Troyan, E. E. Clothiaux, E. L. Mlawer, and G. G. Mace, 2003: ARM value-added cloud products: description and status. [Available online at http:// www.arm.gov/publications/proceedings/ conf13/ extended_ abs/miller-ma.pdf.]

Moran, K. P., B. E. Martner, M. J. Post, R. A. Kropfli, D. C. Welsh, and K. B. Widener, 1998: An unattended cloud-profiling radar for use in climate research. *Bull. Amer. Meteor. Soc.*, **79**, 443–455.

Plana-Fattori, A., and Coauthors, 2009: Comparison of high-cloud characteristics as estimated by selected spaceborne observations and ground-based lidar datasets. *Journal of Applied Meteorology and Climatology*, **48**, 1142–1160.

Protat, A., and Coauthors, 2009: Assessment of CloudSat reflectivity measurements and ice cloud properties using ground-based and airborne cloud radar observations. *J. Atmos. Oceanic Technol.*, **26**(9), 1717–1741.

Protat, A., and Coauthors, 2014: Reconciling ground-based and space-based estimates of the frequency of occurrence and radiative effect of clouds around Darwin, Australia. *Journal of Applied Meteorology and Climatology*, **53**, 456–478, doi: 10.1175/JAMC-D-13-072.1.

Qian, Y., C. N. Long, H. Wang, J. M. Comstock, S. A. McFarlane, and S. Xie, 2012: Evaluation of cloud fraction and its radiative effect simulated by IPCC AR4 global models against ARM surface observations. Atmos. Chem. Phys., **12**, 1785–1810, doi: 10.5194/acp-12-1785-2012.

Rossow, W. B., and R. A. Schiffer, 1999: Advances in understanding clouds from ISCCP. *Bull. Amer. Meteor. Soc.*, **80**, 2261–2287.

Sassen, K., and Z. E. Wang, 2008: Classifying clouds around the globe with the CloudSat radar: 1-year of results. *Geophys. Res. Lett.*, **35**, L04805, doi: 10.1029/2007GL032591.

Sassen, K., and Z. E. Wang, 2012: The clouds of the middle troposphere: Composition, radiative impact, and global distribution. *Surveys in Geophysics*, **33**, 677–691, doi: 10.1007/s10712-011-9163-x.

Sherwood, S. C., S. Bony, and J.-L. Dufresne, 2014: Spread in model climate sensitivity traced to atmospheric convective mixing. *Nature*, **505**, 37–42, doi: 10.1038/nature12829.

Stephens, G., 2005: Cloud feedbacks in the climate system: a critical review. *J. Climate*, **18**, 237–273.

Stephens, G., and Coauthors, 2002: The CloudSat Mission and the A-Train: A new dimension of space-based observations of clouds and precipitation. *Bull. Amer. Meteor. Soc.*, **83**, 1771–1790.

Thorsen, T. J., Q. Fu, J. M. Comstock, C. Sivaraman, M. A. Vaughan, D. M. Winker, and D. D. Turner, 2013: Macrophysical properties of tropical cirrus clouds from the CALIPSO satellite and from ground-based micropulse and Raman lidars. *J. Geophys. Res.*, **118**, 9209–9220, doi: 10.1002/jgrd.50691.

Wang, F., S. Yang, and T. W. Wu, 2014: Radiation budget biases in AMIP5 models over the East Asian monsoon region. *J. Geophys. Res.*, **119**, 13 400–13 426, doi: 10.1002/2014JD022243.

Wang, Z. E., and K. Sassen, 2001: Cloud type and macrophysical property retrieval using multiple remote sensors. *J. Appl. Meteor.*, **40**, 1665–1682.

Winker, D. M., W. H. Hunt, and M. J. McGill, 2007: Initial performance assessment of CALIOP. *Geophys. Res. Lett.*, **34**, L19803, doi: 10.1029/2007GL030135.

Xi, B. K., X. Q. Dong, P. Minnis, and M. M. Khaiyer, 2010: A 10year climatology of cloud fraction and vertical distribution derived from both surface and GOES observations over the DOE ARM SPG site. *J. Geophys. Res.*, **115**, D12124, doi: 10.1029/2009JD012800.

Yoo, H, Z. Q. Li, Y. T. Hou, S. Lord, F. Z. Weng, and H. W. Barker, 2013: Diagnosis and testing of low-level cloud parameterizations for the NCEP/GFS model using satellite and ground-based measurements. *Climate Dyn.*, **41**, 1595–1613, doi: 10.1007/s00382-013-1884-8.

Zhang, J. Q., Z. Q. Li, H. B. Chen, H. Yoo, and M. Cribb, 2014: Cloud vertical distribution from radiosonde, remote sensing, and model simulations. *Climate Dyn.*, **43**, 1129–1140, doi: 10.1007/s00382-014-2142-4.

Zhang, M. H., and Coauthors, 2005: Comparing clouds and their seasonal variations in 10 atmospheric general circulation models with satellite measurements. *J. Geophys. Res.*, **110**, D15S02, doi: 10.1029/2004JD005021.

Zhang, Y. Y., and S. A. Klein, 2010: Mechanisms affecting the transition from shallow to deep convection over land: Inferences from observations of the diurnal cycle collected at the ARM Southern Great Plains site. *J. Atmos. Sci.*, **67**, 2943–2959.